J Mol Model (2011) 17:1625–1633
DOI 10.1007/s00894-010-0859-5

ORIGINAL PAPER

The mechanism of methanol decomposition by CuO. A theoretical study based on the reaction force and reaction electronic flux analysis

Maria Luisa Cerón · Barbara Herrera · Paulo Araya · Francisco Gracia · Alejandro Toro-Labbé

Received: 7 July 2010 / Accepted: 23 September 2010 / Published online: 19 October 2010

Abstract A theoretical study of methanol decomposition using a model representing the initial step of the reaction $CH_3OH + CuO \rightarrow CH_2O + H_2O + Cu$ is presented. Theoretical calculations using B3LYP/6-31 G along with Lanl2DZ pseudopotentials on metallic centers were performed and the results discussed within the framework of the reaction force analysis. It has been found that the reaction takes place following a stepwise mechanism: first, copper reduction ($Cu^{+2} \rightarrow Cu^{+}$) accompanies the oxygen transposition and then a second reduction takes place ($Cu^{+} \rightarrow Cu^{0}$) together with a proton transfer that produce formaldehyde and release a water molecule.

Keywords Electronic reaction flux · Methanol decomposition · Reaction force

M. L. Cerón · P. Araya · F. Gracia
Centro de Investigación Interdisciplinaria en Ciencia de los Materiales (CIMAT), Laboratorio de Catálisis, Facultad de Ciencias Físicas y Matemáticas, Universidad de Chile, 8320000 Santiago, Chile

M. L. Cerón
Laboratorio de Química Teórica Computacional (QTC), Facultad de Química, Pontificia Universidad Cat´olica de Chile, 7810000 Santiago, Chile

B. Herrera (✉) · A. Toro-Labbé
Centro de Investigación Interdisciplinaria en Ciencia de los Materiales (CIMAT), Laboratorio de Química Teórica Computacional (QTC), Facultad de Química, Pontificia Universidad Católica de Chile, 7810000 Santiago, Chile
e-mail: bherrera@uc.cl

Introduction

Currently, environmental reasons made necessary the replacement of fossil fuels by new sources of renewable energy. Among the current alternatives of energy the use of fuel cells is an attractive way of using hydrogen in energy production [1]. Among the many liquids considered for generating hydrogen, methanol is the best choice, it is the third chemical commodity after ethylene and ammonia, and is produced from non-renewable or renewable sources like natural gas, oil, fossil, coal, or biomass [2, 3]. The flexibility of conversion of fuel sources to methanol, as well as the catalytic decomposition, steam reforming, partial oxidation and oxidative steam reforming (which is a combined process of reforming) are very studied reactions due to the importance and their cost on hydrogen production [3–5]. These reactions can be catalyzed by metals supported on oxides, the most used are SiO_2, ZrO_2, CeO_2 and Al_2O_3 [3–6]. Experimentally, the activity of Cu/ZrO_2 has been discussed widely [7, 8] due to the favorable interaction that copper offers, creating acidic sites and changing the oxidative state of copper under mild conditions. Additionally, it is known by now that oxidative states of copper play an important role in the hydrogen generation from methanol [7–9], the intermediate formation of Cu^{+} as an active species in the methanol steam reforming, has been observed by temperature programmed reduction (TPR) studies in $CuO/ZnO/ZrO2$ systems, [8] in this context elucidate the role of copper in this catalytic process is important and a very difficult task. To establish which are the copper active species in the methanol decomposition a simplified context in which the reaction takes place in gas phase is assumed.

In this paper the reaction $CH_3OH + CuO \rightarrow CH_2O + H_2O + Cu$ is analyzed from the new perspective provided

by reaction force analysis [10–19], this involves the characterization of different properties along the reaction coordinate. Among these properties, the reaction electronic flux [12, 22] emerged as a good descriptor of the electronic activity taking place during the reaction thus helping elucidate the main features on the methanol decomposition mechanism [10–19]. The electronic activity, being phenomenologically associated with electronic polarization and transfer effects, will be rationalized in terms of chemical events, bond formations and/or strengthening and bond breaking and/or weakening, that occur at different steps of the reaction, this produces a precise characterization of the electronic activity during the chemical reaction.

This article is organized as follows: Section 2 presents the theoretical elements for analyzing the reaction; Section 3 describes the computational methods employed; in Section 4 the results are presented and discussed; in Section 5, a few concluding remarks are drawn.

Theoretical background

Energy and force profiles

The energy profile E(ξ) along a intrinsic reaction coordinate (IRC=ξ) [23] describes the energy change when reactants (**R**) are transformed into products (**P**) passing by a transition state (**TS**). Although the energy profile provides the thermodynamic and kinetic information of an elementary step, it does not give insights on the reaction mechanism, which is related with the nuclear displacements and electronics reordering that takes place when the reactants are transformed into products [11–14, 24, 25]. The reaction force analysis provides the framework to characterize the mechanism of the reaction, it is defined as [10–19]:

$$\mathrm{F}(\xi) = -\frac{\mathrm{dE}(\xi)}{\mathrm{d}\xi}. \tag{1}$$

In general a generic elementary step, the reaction force profile defines three reaction regions, delimited by the minimum and maximum of the profile [13, 14, 24]. In the reactant region ($\xi_R \leq \xi \leq \xi_{min}$) structural changes prepares the reactants for continuing the reaction; the transition state region ($\xi_{min} < \xi < \xi_{max}$) is where most bond forming and breaking process are observed; in the product region ($\xi_{max} \leq \xi \leq \xi_P$), structural relaxation leads to the products. As the reactant region, the product region is mainly characterized by structural changes [13, 14, 25].

One of the most important results that comes out from the definition of reactions regions is a rational partition of the activation and reaction energies, [17–19] $\Delta E^{\neq}$ and ΔE^{0}, respectively:

$$\Delta \mathrm{E}^{\neq} = \mathrm{W}_1 + \mathrm{W}_2;\ \Delta \mathrm{E}^{\circ} = \mathrm{W}_1 + \mathrm{W}_2 + \mathrm{W}_3 + \mathrm{W}_4 \tag{2}$$

with

$$\mathrm{W}_1 = -\int_{\xi R}^{\xi_{\min}} F(\xi)d\xi > 0 \quad \mathrm{W}_2 = -\int_{\xi \min}^{\xi_0} F(\xi)d\xi > 0 \tag{3}$$

$$\mathrm{W}_3 = -\int_{\xi 0}^{\xi_{\max}} F(\xi)d\xi < 0 \quad \mathrm{W}_4 = -\int_{\xi \max}^{\xi p} F(\xi)d\xi < 0\,. \tag{4}$$

Where ξ_0 denotes the position of the transitions state. It is important to stress the fact that Eq. 2 reveals the physical nature of the activation energy.

Chemical potential and reaction electronic flux

The chemical potential (μ) is a global electronic property that within the frame of density functional theory (DFT), describes the reactivity of molecular systems since it measures the escaping tendency of electrons from equilibrium [26–29]. For an N - electron system with total energy E and external potential $\upsilon(\boldsymbol{r})$, the chemical potential, is defined as [26]

$$\mu \approx \left(\frac{\partial E}{\partial N}\right)_{\upsilon(\mathrm{r})} = -x \tag{5}$$

where x is the electronegativity [26–29]; Using a finite difference approximation and the Koopmans [19, 20] (or Janack [21]) theorems, the chemical potential can be estimated through the following formula [26, 27, 30]:

$$\mu \approx -\frac{1}{2}(\mathrm{I} + \mathrm{A}) \approx \frac{1}{2}(\varepsilon_{\mathrm{L}} + \varepsilon_{\mathrm{H}}), \tag{6}$$

where I and A are the ionization potential and electronic affinity; ε_H and ε_L are the energies of the highest occupied and lowest unoccupied molecular orbitals, HOMO and LUMO, respectively. Note that through the use of Eq. 6 μ can be determined numerically all along the reaction coordinate, thus giving rise to a chemical potential profile $\mu(\xi)$.

For a complete description of the electronic activity along the reaction coordinate the reaction electronic flux (REF) [12] has been recently introduced, it is the derivative of the chemical potential with respect to the reaction coordinate:

$$J(\xi) = -\mathrm{Q}\frac{d\mu}{d\xi}, \tag{7}$$

where Q is the transport coefficient; although in some special cases it can be calculated from values of activation

and reaction energies and chemical potential, [24, 25] Q=1 will be used throughout this paper to allow a correct comparison of the different processes involved in the methanol decomposition reaction. The reaction electronic flux is a new descriptor that identifies and characterizes the electronic activity that takes place during the reaction. Analogy with chemical thermodynamics indicates that $J(\xi)>0$ will be associated with spontaneous reordering of electron density whereas non-spontaneous electronic reordering is expected in region where $J(\xi)<0$. On the other hand, when $J(\xi)>0$ the electronic activity is mostly due to bond formation processes whereas when $J(\xi)<0$ the bond breaking processes are driving the reaction.

The REF can be decomposed into two contributions: polarization $J_p(\xi)$ and transfer $J_t(\xi)$, such that [22]:

$$J(\xi) = J_p(\xi) + J_t(\xi) \tag{8}$$

The polarization flux is due to the electronic reordering occurring within a reacting fragment induced by the presence of the nearby partner fragments. In this context, the whole system, represented by a supermolecule, is partitioned into n_f fragments such that the polarization flux can be written as:

$$J_p(\xi) = \sum_{i=1}^{n_f} J_i(\xi), \tag{9}$$

with

$$J_i(\xi) = -Q_i \frac{d\mu_i}{d\xi} \tag{10}$$

where $J_i(\xi)$ is interpreted as the polarization flux in fragment i due to the presence of the remaining $(n_f - 1)$ moieties that polarize it. The calculation of $J_i(\xi)$ can be achieved by using the counterpoise method [34] that allows fragmentation of any molecular system all along the reaction coordinate and taking Q_i=1 for all fragments. The flux associated to electronic transfer is then given by,

$$J_t(\xi) = J(\xi) - J_p(\xi) = J(\xi) - \sum_{i=1}^{n_f} J_i(\xi) = -\frac{d}{d\xi}\left[\mu - \sum_{i=1}^{n_f} \mu_i\right] \tag{11}$$

In this way the nature of the electronic activity along ξ can be associated to polarization and transfers effects, the balance of these effects defines the fingerprint of the actual reaction mechanism.

REF and electronic population

Within the DFT context, the REF can be linked to the sum of derivatives of bond populations associated to the reactive core of the fragments involved in the reaction [33]. Recalling the chemical potential expressed in terms of Fukui function[23, 32] and then condensing it conveniently to atoms or diatoms, [31] leads to:

$$\mu = \int f(r)\delta v(r)dr \Rightarrow \mu \sim \sum_k v_k \cdot f_k \tag{12}$$

Using the local density approximation for the Fukui fuction, $f_k = \frac{\rho_k}{N}$, [31] the following expression for the reaction electronic flux emerges

$$J(\xi) = -Q\frac{d\mu}{d\xi} \cong -\frac{Q}{N}\sum_k \frac{d}{d\xi}(v_k \cdot \rho_k) \cong -\frac{Q}{N}\sum_k \left(\frac{dv_k}{d\xi}\right) \cdot \rho_k - \frac{Q}{N}\sum_k v_k \cdot \left(\frac{d\rho_k}{d\xi}\right). \tag{13}$$

Now, assuming that the external potential v_k associated to atom or diatom k remains constant along ξ, this is a reasonable approximation since the chemical nature of the integration basins used to condensate the properties is not expected to change during the reaction, then the first term of the right hand side of Eq. 13 vanishes, leading to:

$$J(\xi) = -\frac{Q}{N}\sum_k v_k \cdot \left(\frac{d\rho_k}{d\xi}\right) \tag{14}$$

Therefore the REF appears to be proportional to the sum of derivatives of condensed electronic populations weighted by the external potential v_k. This will be quite useful for linking the global polarization and transfer effects to electronic activity observed in specific atoms and bonds within the reactive core of the fragments.

Computational details

All calculations were performed at the B3LYP level [35] with standard 6-31G basis set and Lanl2DZ pseudopotential [36–38] on copper. The transition states were determined through the quadratic synchronous transit (QST3) methodology [39] and a quasi-Newton algorithm to complete the optimization. The reactants, transition state and products were fully characterized by frequency calculations. The path of minimum energy between reactants and products

were calculated through the intrinsic reaction coordinate procedure (IRC) [23]. The reaction force was obtained through numerical differentiation of the energy profile. Using the optimized geometries obtained from the IRC procedure, single point calculations were performed to obtain the profiles of chemical potential and reaction electronic flux. The Mulliken electronic population analysis were then used to make the bridge between REF and electronic activity associated to specific atomic centers. All calculation were performed using the Gaussian 03 (revision D.02) [40] package.

The REF decomposition follows an arbitrary fragmentation of the supermolecular system, this is actually suggested by the transition state structure and numerically implemented through the use of the counterpoise method [34] in Gaussian 03. The counterpoise routine, is often used to determine the basis set superposition error (BSSE) [34] in molecular interactions calculations, however, in the present situations it allows to calculate isolated fragments at each point along ξ using the geometry they have in the supermolecular array. In this way, individual values of chemical potential are determined along the reaction coordinate that produce the corresponding polarization fluxes according to Eq. 9. The resulting individual fluxes are interpreted as polarization due to the presence of the other fragments, although it is important to note that individual polarization fluxes allow electronic transfer within the fragments.

Results and discussion

Energy and reaction force

Figure 1 illustrates the reaction of methanol decomposition induced by *CuO*. In the first step, **R** → **TS** → **MSI**, methanol interacts with *CuO* producing a metastable intermediate $CuO\cdots CH_3^+ + OH^-(MSI)$. This step presents an energy barrier of about 40 kcal/mol and the **MSI** was found at about 10 kcal/mol above the reactant, see Table 1. The second step **MSI** → **QTS** → **P** involves a hydrogen transfer from methanol to the hydroxy ion to form formaldehyde, detached from Cu, and the release of a water molecule. The observed copper reduction in this mechanism, is consistent with experimental data [8] thus assigning some degree of reliability to the simplified model. A qualitative confirmation of the important role of the copper reduction processes along the reaction coordinate can be obtained through the analysis of the evolution of the Mulliken charges on the copper atom, as shown in Fig. 2. It can be observed an initial reduction to reach Cu^+ that catalysis the oxygen transposition; then copper recovers its original oxidation state to finally have a reduction process to Cu^0. Figure 3a shows the energy profile along ξ, where it is possible to observe a transition state **TS** and a quasi-transition state **QTS**, which is not properly an energy maximum although at the current level of calculation it presents a unique imaginary frequency, signature of a transition state. The transformation of **R** into **P** is better understood through the use of the reaction force analysis. Five reaction regions along ξ can be identified in Fig. 3b, these are: reactant (**R**), transition state (**TS**), metastable intermediate (**MSI**), quasi-transition state (**QTS**) and product (**P**). The decomposition of the activation energy in the first step of the reaction shows that $W_1 = 0.63\Delta E^{\neq}$ and $W_2 = 0.37\Delta E^{\neq}$ indicating that structural rearrangements are actually driving the first step of the reaction. In the **R** region, the reactants are prepared through structural rearrangements in order to activate the adsorption of methanol; the energy necessary for this process is W_1= 25.49 kcal/mol. At the **TS** region the work required to reach the transition state for the oxygen transposition, a S_N2 type reaction, at the methyl molecular plane is given by W_2= 15.13 kcal/mol. In summary, 63% of the activation energy produces structural rearrangements to bring the separated molecules into the right position to achieve the methyl interaction with *CuO*; The remaining 37% of the activation energy is responsible for the cleavage of the $C-O(H)$ bond and the formation of the $C-O(Cu)$ bond, this is agreement with other results obtained in our group [12, 22].

Table 1 summarizes the energy data involved in each of the processes defined within the five reaction regions.

The reaction electronic flux

HOMO and LUMO energies were used to calculate the μ profile displayed in Fig. 4a. It can be noticed that μ is practically constant at the reactant and **MSI** regions and presents a minimum at the **TS** region. This suggest that the oxygen transposition is at least at the first stages of the reaction, weakly assisted by electronic reordering. When entering the **QTS** region, there is a strong change in μ, indicating that the proton transfer that takes place in this step is assisted by a large electronic activity; then μ steadily increases until reaching a plateau at the product region.

Figure 4b displays $J(\xi)$, obtained from Eq. 7 with Q=1. At the reactant region a fluctuating zero flux regime, associated to equilibrium states, dominates the picture, this is only disrupted in the the **TS** region by a positive pulse followed by a negative peak, thus confirming the electronic activity already observed in Fig. 4a. Then at the **MSI** region again there is a zero flux zone that is in turn disrupted by a negative broad peak developed at the **QTS** region that is maintained until the P region; this is evidence that the reaction mechanism is stepwise and most electronic activity take place first at the **TS** and then at the **QTS** and products

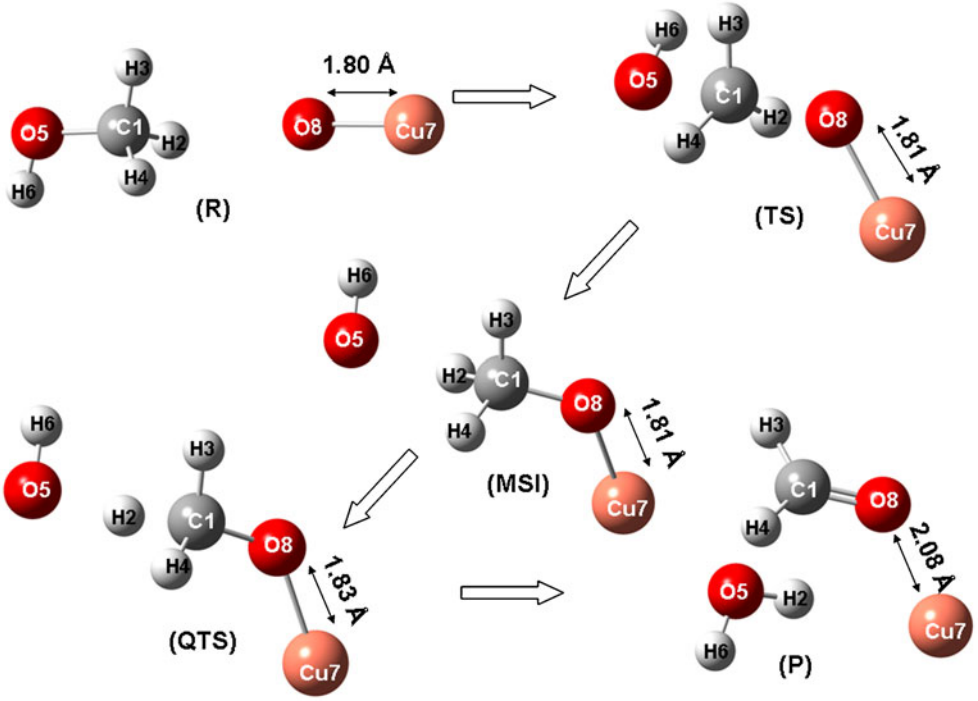

Fig. 1 Scheme of methanol decomposition with *CuO*

regions. In order to get details on the nature of the electronic flux it is convenient to analyze separately $J_p(\xi)$ and $J_t(\xi)$.

Fragmentation of the supermolecule As already mentioned, the decomposition of the overall electronic flux in $J_p(\xi)$ and $J_t(\xi)$, allows one to explain the nature of the electronic activity in terms of polarization and transfers effects [22]. Note that when evaluating the influence of $J_p(\xi)$ and $J_t(\xi)$ in $J(\xi)$ it is necessary a careful analysis of the development of each contribution, associating the shape of $J(\xi)$ to specific trends appearing in $J_p(\xi)$ and/or $J_t(\xi)$. This identifies the type of flux that is mainly observed in a given step.

The structure of the transition state is shown in Fig. 5, it can be observed that three main fragments can be easily distinguished. In this context a partition of three fragments, n_f=3 in Eq. 11, as suggested by the transition state structure, was used within the *counterpoise* method [34] in order to analyze the polarization electronic flux of each fragment all along the reaction coordinate. For the three fragments, we have evaluated $\mu(\xi)$ and $J_p(\xi)$, obtaining $J_t(\xi)$ from Eq. 11, the results are shown in Fig. 6a. It can be observed that most polarization effects are non-spontaneous $J_p(\xi)<0$, they show up at the **TS**, **QTS** and **P** regions and appear to be induced by the mostly spontaneous electron transfer processes mainly observed also in regions **TS**, **QTS** and **P**.

The REF indicates that the reaction evolves from a zero flux regime within the reactant region; by the end of this region and entering the **TS** region, simultaneous polarization and transfer fluxes are observed, the transfer flux dominates the **TS** region thus indicating the presence of bond breaking and forming processes. The electronic activity observed in the transition state region and depicted through a negative peak in Fig. 4b can now be identified as being due to transfer processes. Note in Fig. 6b that polarization effects on the fragments are not very intense in the first three regions, as they appear within the **QTS** and **P** regions where a large polarization of fragment 1 is observed. Moreover, it is the polarization of fragment 1 due to the nearby presence of the other two fragments that dominates the polarization effects.

It can be observed in Fig. 6a that in the **MSI** region $J_p(\xi)$ and $J_t(\xi)$ fluxes remain quite constant but entering the **QTS**

Table 1 Works involved at the different local process along ξ for the decomposition of methanol using copper (II) oxide. All work were calculated at B3LYP level using pseudo- potential LanL2DZ at heavy atoms

Process	ΔE°	$\Delta E^{\neq}$	W_1	W_2	W_3	W_4	W_5	W_6
R → TS → MSI		40.62	25.49	15.13	-11.89	-23.51		
MSI → QTS → P						-23.51	-6.31	-27.96
Overall Reaction	-29.05	40.62	25.49	15.13	-11.89	-23.51	-6.31	-27.96

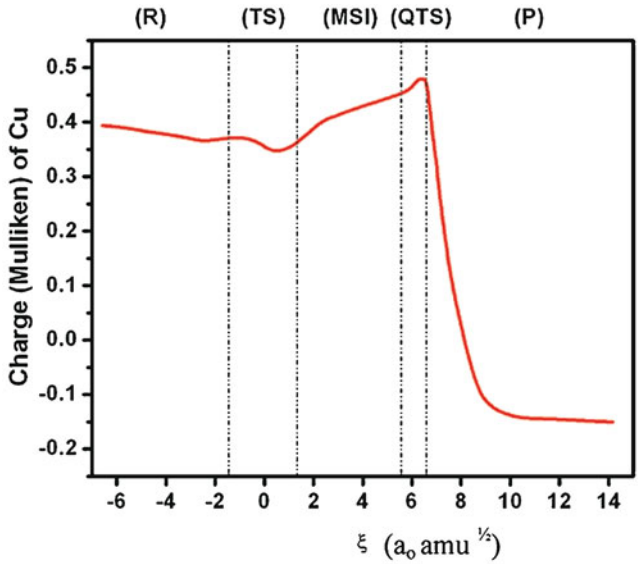

Fig. 2 Mulliken charge of Cu along ξ

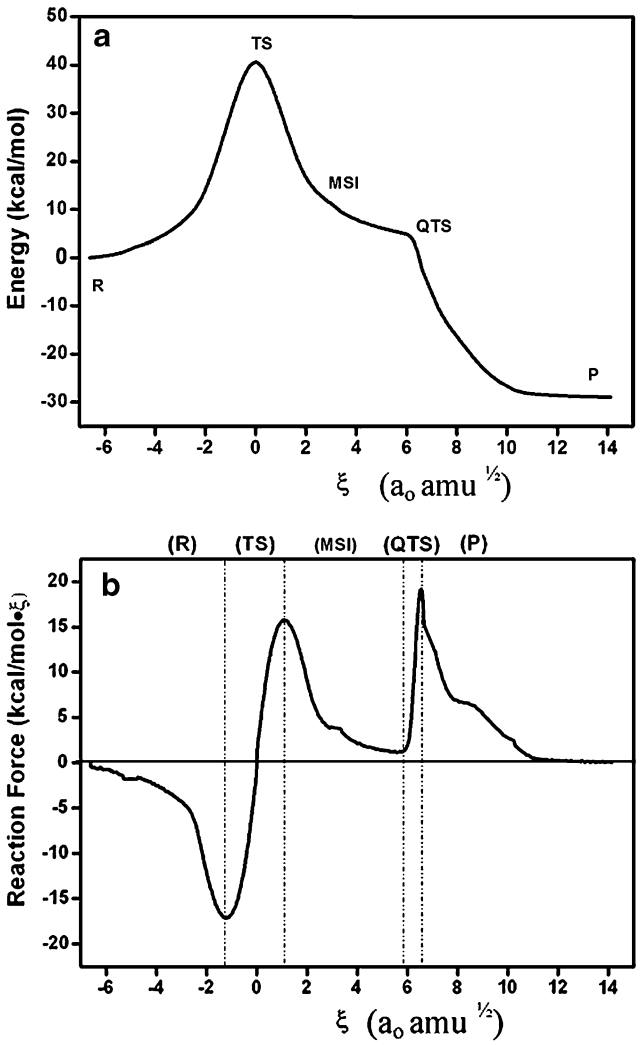

Fig. 3 **a** Energy profile, **b** reaction force profile for the methanol decomposition with *CuO*

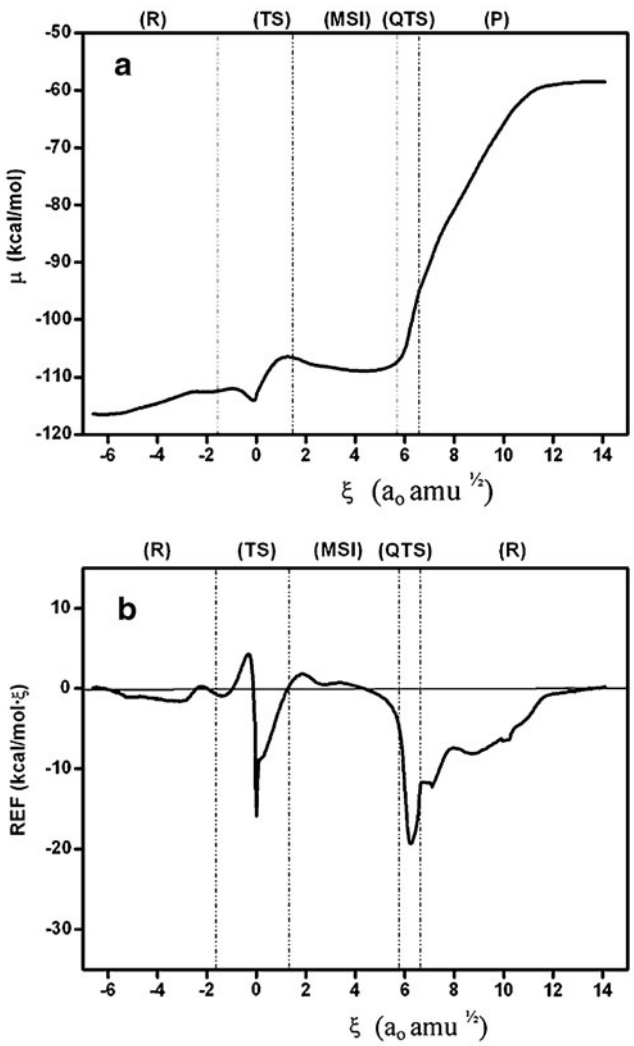

Fig. 4 **a** Chemical potential profile, and **b** REF profile along ξ for the methanol decomposition with *CuO*

region $J_p(\xi)$ drives the reaction until the products is reached, compare the electronic activity observed in Figs. 4b and 6. Clear evidence indicates that the reaction electronic flux at the second step of the reaction is mostly due to polarization emerges, although electron transfer also plays and important role in the formaldehyde formation. In the next Section the observed fluxes will be related to bond breaking and forming processes.

Electronic bond population analysis

To confirm the above findings, we have carried out a Mulliken population analysis to identify the representative atoms and bonds responsible for the electronic activity. Figure 7a displays the evolution of the bond electronic populations involving O8 with its donor and acceptor atoms

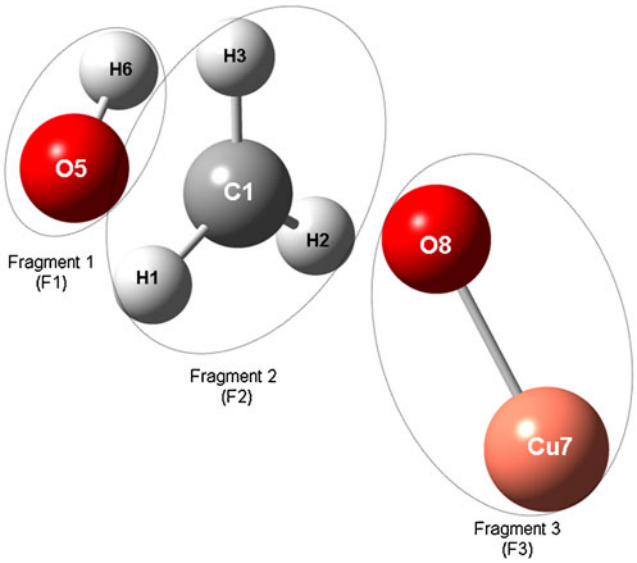

Fig. 5 Fragmentation of the supermolecule suggested by **TS** structure to calculate J_p and J_t

and the cleavage of the C1O5 bond (ρ_{C1O5}, ρ_{C1O8}; ρ_{O8Cu}), see Fig. 1 for the atomic labels. The three electronic populations within **R** remains quite constant, confirming that the activation of the oxygen transposition needs first a structural reordering. At **TS**, ρ_{C1O5} decrease rapidly indicating that this bond breaks within the **TS** region; ρ_{C1O8} presents a strong increase due to the formation of the single bond, both populations cross each other at the transition state. This electronic activity is consistent with the electronic transfer observed in Figs. 4 and 6 through the reaction electronic flux analysis within the **TS** region, ρ_{C1O8} remain practically constant at **MSI** and **QTS** regions, in the latter it crosses with ρ_{O8Cu}, that follows an opposite trend. The double bond formation of the aldehyde and the copper reduction processes are achieved within the product region, the electronic transfer and polarization involved in such processes are observed in Fig. 6a. These results confirm that the C1O5 bond cleavage and C1O8 bond forming are responsible for the transfer peak observed in Figs. 4 and 6a. As already mentioned, the O8Cu7 bond population remains quite constant until leaving the **QTS** region where the bond breaks down, this indicates that the proton transfer is not affected by the oxygen exchange that takes place earlier, at the **TS** region.

Figure 7c shows the bond electronic populations involved in the proton transfer: ρ_{C1H2} and ρ_{O5H2}. The populations show the O5H2 bond formation and C1H2 bond cleavage that allows the water release observed in the product region. Note that these populations only change slightly in the first three region although it is clear that the process initiates at the **TS** region where a first change in the slopes of the population profiles is observed. The new trend is maintained until the **QTS** region when the O5H2 and C1H2 populations drastically change. Then at the products region, it is evident that the O5H2 bond has been formed whereas the C1H2 bond has been broken down. It seems that once reached the **TS** molecular vibrations assist the methyl's hydrogen to generate a water molecule. Overall, the chemical events analyzed so far indicate that breaking bond processes drive the reaction at the **QTS** and products regions.

Let us now analyze the derivatives of bond populations along the reaction coordinate (see Fig. 7b and d), this shows the rates of dissociation and formation of the respective bonds. Bond breaking process are associated with negative values of the derivative whereas positive values indicate bond formation. Figure 7b and d confirms that regions **TS**,

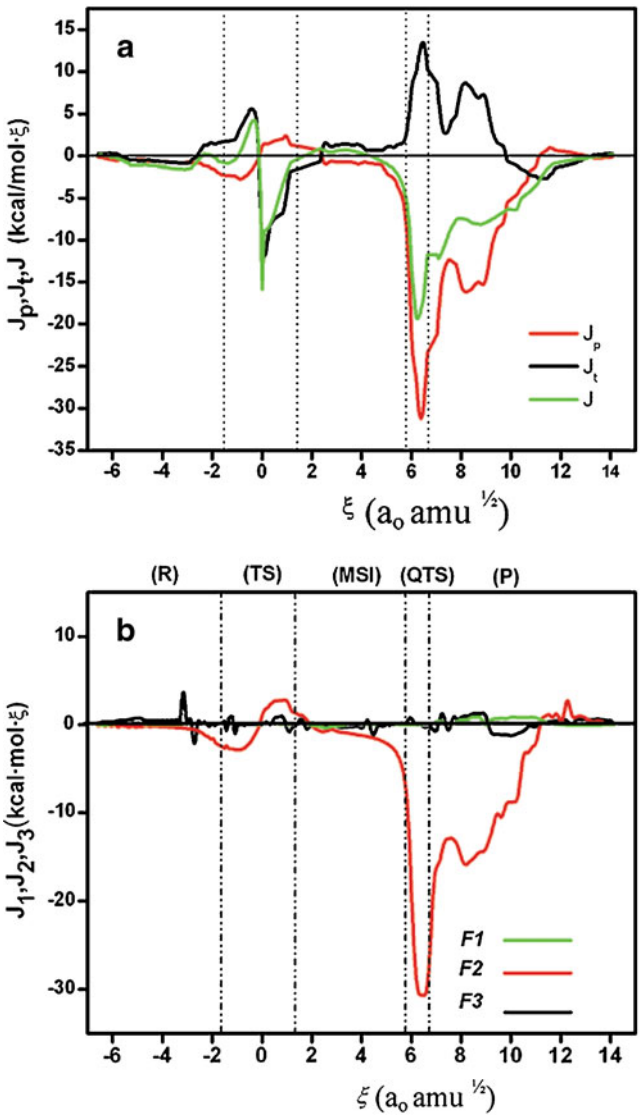

Fig. 6 **a** Polarization and transfer contributions to the REF **b** Contributions of individuals fragments to the polarization flux

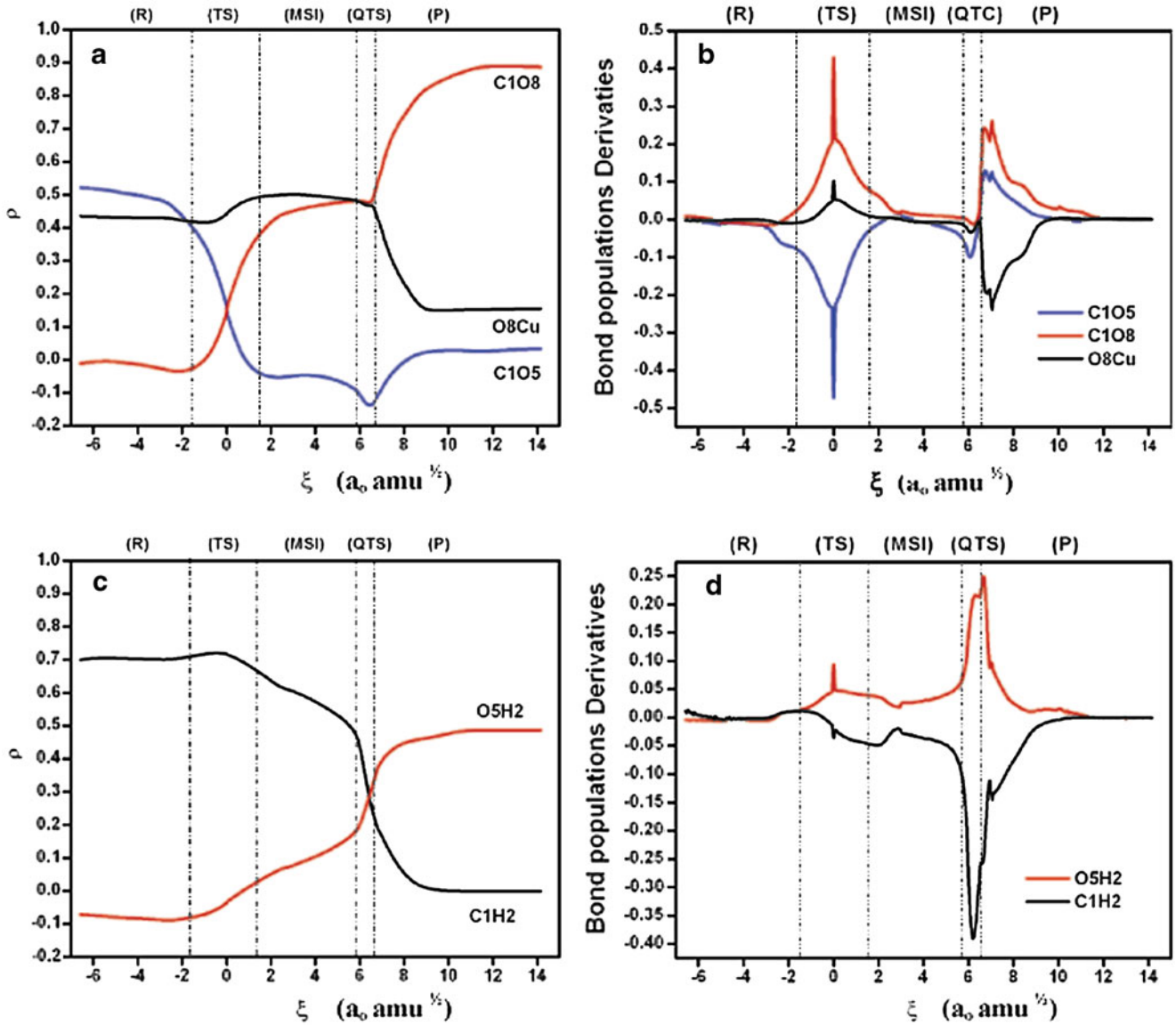

Fig. 7 Mulliken bond populations involved in: (**a**) the exchanged oxygen and (**c**) the proton transfer. (**b**) and (**d**) are bond population derivatives

QTS and **P** show the most intense electronic activity. The positive peak observed at the **TS** region shows the C1O8 bond formation whereas the negative peak is according to the C1O5 bond cleavage. On the other hand, at the **QTS** region positive peaks reveal the formation of the O5H2 bond and C1O8 double bond; negative peaks are fingerprints for the O8Cu7 and C1H2 bonds breaking. Note that the formation of the single and double C1O8 bonds appears localized at the **TS** and **QTS** regions.

Concluding remarks

A detailed analysis of the mechanism of methanol decomposition induced by *CuO* has been presented. Results show that copper reduction is a key step of the reaction. Cu^{+} becomes an active species in the formation of the product formaldehyde. The reaction force analysis of energy barrier indicated that this is mostly due to structural rearrangements, less that 40% of the activation energy can be attributed to pure electronic activity. On the other hand, the electronic activity observed during the reaction was analyzed in terms of the reaction electronic flux, indicating that the reaction proceeds in two steps: (1) copper reduction $Cu^{+2} \rightarrow Cu^{+}$ and oxygen transposition; (2) copper reduction $Cu^{+} \rightarrow Cu^{0}$ and proton transfer this last step produces formaldehyde with the release of a water molecule. Consistency with bond population analysis indicates that the reaction electronic flux a global property of the reaction, is a good descriptor of the electronic activity taking place during the reaction.

Acknowledgements This work was supported by FONDECYT under grants N° 1090460 and N° 11080002, FONDAP Project N° 11980002 (CIMAT). María Luisa Cerón wants to thank Santander-Universia for a Doctoral fellowship and Beca de apoyo a la realización de tesis doctoral-Conicyt.

References

1. Lindström B, Petterson LJ (2001) Int J Hydrogen Energy 26:923–933
2. Jacobs G, Davis BH (2005) Appl Catal A 285:43–49
3. Cubeiro ML, Fierro JLG (1998) Appl Catal A 168:307–322
4. Agrell J, Birgersson H, Boutonnet M (2002) J Power Sources 106:249–257
5. Velu S, Suzuki K, Kapoor MP, Ohashi F, Osaki T (2001) Appl Catal A 213:47–63
6. Fischer IA, Bell AT (1999) J Catal 184:357–376
7. Ko JB, Bae CM, Jung YS, Kim DH (2005) Catal Letters 105:157–161
8. Oguchi H, Kanai H, Utani K, Matsumura Y, Imamura S (2005) Appl Catal A Gral 293:64–70
9. Sloczyński J, Grabowski R, Kozlowska A, Olszewski PK, Stoch J (2003) Phys Chem Chem Phys 5:4631–4640
10. Toro-Labbé A, Martinez J (2004) Chem Phys Lett 392:132–139
11. Herrera B, Toro-Labbé A (2004) J Phys Chem 121:7096–7102
12. Herrera B, Toro-Labbé A (2007) J Phys Chem A 111:5921–5926
13. Toro-Labbé A, Gutiérrez-Oliva S, Concha MC, Murray JS, Politzer P (2004) J Phys Chem 121:4570–4576
14. Politzer P, Toro-Labbé A, Gutiérrez-Oliva S, Herrera B, Jaque P, Concha MC, Murray JS (2005) J Chem Sci 117:467–472
15. Gutiérrez-Oliva S, Herrera B, Toro-Labbé A, Chermette H (2005) J Phys Chem A 109:1748–1751
16. Politzer P, Burda JV, Concha MC, Lane P, Murray JS (2006) J Phys Chem A 110:756–761
17. Rincón E, Jaque P, Toro-Labbé A (2006) J Phys Chem A 110:9478–9485
18. Burda JV, Murray JS, Toro-Labbé A, Gutierrez-Oliva S, Politzer P (2009) J Phys Chem A 113:6500–6503
19. Burda JV, Murray JS, Toro-Labbé A, Gutierrez-Oliva S, Politzer P (2007) J Phys Chem A 111:2455–2458
20. Parr RG, Zhou Z (1993) Acc Chem Res 26:256–258
21. Janak JF (1978) Phys Rev B 18:7165–7168
22. Echegaray E, Toro-Labbé A (2008) J Phys Chem A 112:11801–11807
23. Fukui K (1981) Acc Chem Res 14:363–368
24. Toro-Labbé A (1999) J Phys Chem A 103:4398–4403
25. Jaque P, Toro-Labbé A (2000) J Phys Chem A 104:995–1003
26. CK JKS (1987) Electronegativy: structure and bonding, 66. Berly, Germany
27. Pearson R (1985) J Am Chem Soc 107:6801–6806
28. Pauling L (1960) The nature of chemical bond. Cornell University Press, Ithaca, NY
29. Ayers PW, Parr R (2000) J Am Chem Soc 122:2010–2018
30. Geelings P, De Proft F, Langenaeker W (2003) Chem Rev 103:1793–1874
31. Yang W, Mortier WJ (1986) J Am Chem Soc 108:5708–5711
32. Fukui K (1970) J Phys Chem 74:4161–4163
33. Vogt-Geisse S, Toro-Labbé A (2009) J Chem Phys 130:244308-244315
34. Simon S, Duran M, Dannenberg JJ (1996) J Chem Phys 105:11024–11031
35. Becke A (1993) J Chem Phys 98:5648–5652
36. Hay PJ, Wadt WR (1985) J Chem Phys 82:270–283
37. Hay PJ, Wadt WR (1985) J Chem Phys 82:284–298
38. Hay PJ, Wadt WR (1985) J Chem Phys 82:299–310
39. Ayala PY, Schlegel HB (1997) J Chem Phys 107:375–384
40. Frisch MJ, Trucks GW, Schlegel HB, Robb MA, Cheeseman JR, Montgomery JA, Vreven T, Kudin KN, Burant JC, Millam JM, Tomasi J, Barone V, Mennucci B, Cossi M, Scalmani G, Rega N, Petersson GA, Nakatsuji H, Hada M, Ehara M, Toyota K, Fukuda R, Hasegawa J, Ishida M, Honda Y, Kitao O, H. Nakai, M. Klene, X. Li, Knox JE, Hratchian HP, Cross JB, Bakken V, Adamo C, Jaramillo J, Gomperts R, Stratmann RE, Yazyev O, Austin AJ, Cammi R, Pomelli C, Ochterski JW, Ayala PY, Morokuma K, Voth GA, Salvador P, Dannenberg JJ, Zakrzewski VG, Dapprich S, Daniels AD, Strain MC, Farkas O, Malick DK, Rabuck AD, Raghavachari K, Foresman JB, Ortiz JV, Cui Q, Baboul AG, Clifford S, Cioslowski J, Stefanov BB, Liu G, Liashenko A, Piskorz P, Komaromi I, Martin RL, Fox DJ, Keith T, Al-Laham MA, Peng CY, Nanayakkara A, Challacombe M, Gill PMW, Johnson B, Chen W, Wong MW, Gonzalez C, Pople JA (2004) Gaussian 03, revision C.02; Gaussian Inc.: Wallingford, CT